Quantum microwaves / Micro-ondes quantiques

Quantum Zeno dynamics in atoms and cavities

Dynamique de Zénon quantique avec des atomes et des cavités

Sébastien Gleyzes [*], Jean-Michel Raimond

Laboratoire Kastler Brossel, Collège de France, CNRS, ENS–PSL Research University, UPMC–Sorbonne Universités, 11, place Marcelin-Berthelot, 75005 Paris, France

A B S T R A C T

Quantum Zeno Dynamics restricts the evolution of a system in a tailorable subspace of the Hilbert space by repeated measurements of a proper observable. This restricted dynamics can be counterintuitive and lead to the generation of interesting nonclassical states. We describe an experiment implementing the Zeno dynamics in an atomic Rydberg level manifold, and we propose an implementation in the cavity quantum electrodynamics context. Both systems open promising perspectives for quantum-enabled metrology and decoherence studies.

© 2016 Published by Elsevier Masson SAS on behalf of Académie des sciences. This is an open access article under the CC BY-NC-ND license (http://creativecommons.org/licenses/by-nc-nd/4.0/).

R É S U M É

La dynamique de Zénon quantique permet de confiner l'évolution d'un système à un sous-espace choisi de son espace de Hilbert par la mesure répétitive d'une observable convenable. Cette dynamique restreinte peut être très contre-intuitive et conduire à la préparation d'états non classiques. Nous décrivons une expérience réalisant cette dynamique dans une multiplicité de Rydberg et proposons une méthode pour l'observer dans le contexte de l'électrodynamique quantique en cavité. Dans les deux cas, la dynamique de Zénon ouvre des perspectives intéressantes pour la métrologie quantique et l'étude de la décohérence.

© 2016 Published by Elsevier Masson SAS on behalf of Académie des sciences. This is an open access article under the CC BY-NC-ND license (http://creativecommons.org/licenses/by-nc-nd/4.0/).

1. Introduction

Fundamental quantum physics is the focus of an intense, worldwide experimental interest, based on techniques making it possible to realize some of the thought experiments designed by the founding fathers. We now trap and manipulate individual quantum systems, ions, atoms, superconducting circuits a.s.o. With them, we witness fundamental quantum behaviors and check our understanding of the quantum world. We also explore the intriguing limit between the quantum and classical worlds. Why the weirdest quantum features are confined at the microscopic scale is yet mainly an open ques-

---

tion [1]. Finally, the ability to tailor complex quantum states opens perspectives for quantum information transmission and processing [2], for quantum simulation of complex systems [3–5], and for quantum-enabled metrology [6].

Cavity quantum electrodynamics (CQED) [7] is representative of this active trend. It implements the simplest matter–field coupling situation, with a single two-level atom coupled with a single mode of the radiation field. CQED has already a long history, starting from the seminal remark by Purcell [8] that atomic spontaneous emission can be tailored by coupling the atom to a resonator. It now focuses on the strong coupling regime, when the coherent coupling of the atom with the mode overwhelms the dissipative processes. In the optical domain, it provides a convenient interface between flying photonics qubits and trapped atoms [9]. In the solid-state realm, it leads to integrated, controllable photon sources [10]. In the microwave domain, with experiments based either on Rydberg atoms [7] or on superconducting circuits [11], it leads to the generation and manipulation of states at the quantum-classical boundary, and to explorations of the decoherence process [12,13].

In most CQED experiments, the final quantum state is reached by tailoring the atom–cavity interaction. For instance, the production of a "Schrödinger cat state", quantum superposition of two coherent fields with different classical phases, can be achieved in microwave CQED by letting a single circular Rydberg atom, initially prepared in a state superposition, interact in the nonresonant, dispersive regime with a coherent field contained in a superconducting cavity [12]. The final state is selected by tuning the initial field, the atom–cavity detuning and the interaction time.

Quantum Zeno Dynamics [14] offers a new route towards non-classical states by tailoring the structure of the Hilbert space instead of the interaction Hamiltonian. It generalizes the Quantum Zeno Effect (QZE) [15]. In the QZE, the coherent evolution of the system is blocked by frequently repeated measurements of an observable admitting the initial state as a non-degenerate eigenstate. In the short time interval between measurements, the system's state changes by an infinitesimal amount. A new measurement thus almost certainly projects the system back onto its initial state, canceling the effect of the coherent evolution. QZE has been observed on a variety of spin-1/2-like systems [16–18]. It has also been observed for the coherent displacement of a cavity field under the action of a classical source [19]. Repeated Quantum Non Demolition measurements of the photon number freeze the system in its initial vacuum state.

QZD leaves more freedom to the system. The initial state then belongs to a multidimensional eigenspace of the repeatedly measured observable. The system evolution is confined into this eigenspace, driven by the restriction of the system's Hamiltonian. By properly choosing the observable, one can tailor the structure of the accessible Hilbert space. This procedure leads in particular to a deterministic preparation of nonclassical states [20,21]. It can also be used for decoherence control [22], state purification [23], and quantum gate implementation [24].

We discuss here a proposal for the implementation of QZD using the tools of microwave CQED [20,21]. We show that it leads to the deterministic generation of cat states and to an efficient state-synthesis procedure. We also describe the first implementation of QZD in a high-dimensional Hilbert space [25], using a Rydberg level Stark manifold, which can be viewed as a quantum simulation of the CQED proposal. It generates nonclassical atomic states, with possible applications in quantum-enabled metrology.

2. Quantum Zeno dynamics in microwave CQED

The principle of the proposed QZD is to repeatedly ask the cavity field: "do you contain exactly s photons?", by measuring the projector $P_s = |s\rangle\langle s|$ on the Fock state $|s\rangle$. This simple question splits the Hilbert space into two parts, the Fock state $|s\rangle$ on the one hand, and, on the other hand, the union of the two subspaces $\mathcal{H}_{<s}$ and $\mathcal{H}_{>s}$ spanned respectively by the Fock states with less or more than s photons.

The coherent evolution is here produced by a classical source coupled with the cavity. Its Hamiltonian is a linear combination of the photon annihilation and creation operators, a and $a^\dagger$ and, therefore, does not couple directly $\mathcal{H}_{<s}$ with $\mathcal{H}_{>s}$. Hence, an evolution starting inside one of these subspaces remains confined in it. The repeated measurement of P_s sets an impenetrable barrier in the Hilbert space. In the phase plane, this barrier can be viewed as an Exclusion Circle (EC), with radius $\sqrt{s}$. In the $s = 1$ case, the EC has a unit radius and blocks the evolution of the vacuum state, implementing the standard QZE [19].

This confined evolution can be rather counterintuitive. Fig. 1 presents the evolution of the field's Wigner function, $W(\xi)$, in the $s = 6$ case, for a stroboscopic evolution in which we alternate small displacements (injected amplitude $\beta = 0.1$) with measurements of P_s. Fig. 1(a) presents 10 snapshots of $W(\xi)$, separated by intervals of five steps. The field starts from $|0\rangle \in \mathcal{H}_{<6}$. Its amplitude first increases along the real axis (free dynamics). Between 15 and 20 steps, the amplitude reaches $\simeq 2$ and QZD comes into play. The coherent state 'collides' on the EC (dashed line in Fig. 1). The field amplitude stops growing and undergoes a progressive π phase-shift between steps 20 and 30. At step 25, the field is in a superposition of two components with opposite phases, a typical cat state. The fringing feature inside the EC is the signature of the quantum coherence of this superposition. At step 35, the field state is nearly coherent with an amplitude close to -2. It then resumes its motion from left to right along the real axis, going through $|0\rangle$ again (around step 45) and heading towards its next 'collision' with the EC.

Fig. 1(b) illustrates QZD in $\mathcal{H}_{>s}$ with an initial coherent state $|\alpha = -5\rangle$. The field collides on the EC after 20 steps. It undergoes a QZD-induced π phase-shift being, at step 25, in a cat state. After 30 steps, the state is again nearly coherent with a positive amplitude. It resumes its motion along the real axis. After 45 steps, its amplitude is slightly larger than 4.5. It would be -0.5 in the case of free dynamics. The QZD-induced phase inversion accelerates the 'propagation' in phase
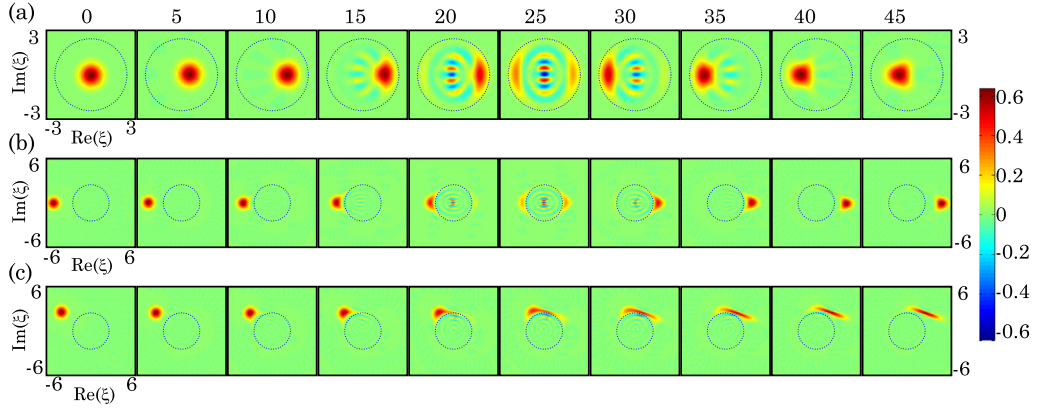
Fig. 1. (a) QZD dynamics in $\mathcal{H}_{<6}$. Ten snapshots of the field Wigner function, $W(\xi)$, obtained after a number of steps indicated above each frame. The cavity is initially in its vacuum state, $s = 6$ and $\beta = 0.1$. The EC is plotted as a blue dashed line. (b) QZD dynamics in $\mathcal{H}_{>6}$. Same as (a) with an initial $\alpha = -5$ amplitude. (c) Same as (b), with an initial amplitude $\alpha = -4 + i\sqrt{6}$. In (b) and (c), the successive frames correspond to the same step numbers as in (a). Reprinted from [20].
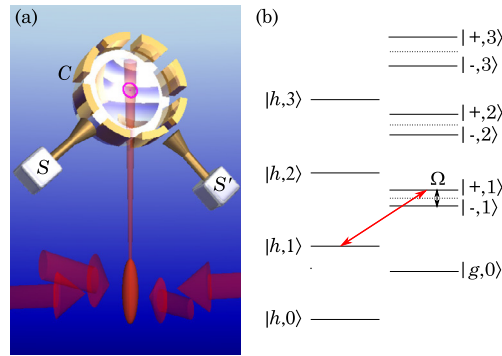
Fig. 2. (a) Proposed experimental scheme. A slow atomic beam extracted from a 2D Magneto-Optical Trap (bottom) forms an atomic fountain. Atoms are nearly at rest in the center of the high-quality microwave Fabry–Perot cavity C (only one mirror shown). Sources S and S′ address respectively the dressed atomic levels and the cavity mode. Electrodes around the cavity mirrors generate the electric fields preparing the circular state shown in the center. (b) Scheme of the dressed atomic levels. The arrow indicates the photon-number selective transition addressed by S for $s = 1$. Reprinted from [20].

space. When the initial amplitude is such that the field state collides tangentially on the EC [Fig. 1(c)], the parts of the Wigner function that come closest to the EC propagate faster than others. The state is distorted and ends up squeezed.

The measurement of P_s can be performed by interrogating the dressed level structure of an atom in the cavity mode. We consider, for the sake of definiteness, a CQED experiment planned at ENS, represented schematically in Fig. 2(a). The superconducting cavity C is resonant at 51.1 GHz. It is coupled with the source S′ driving the coherent field evolution. It is simultaneously probed by a single circular Rydberg atom, prepared inside C [25] out of a slow atomic beam in a fountain arrangement. The transition between the circular levels e (principal quantum number 51) and g (50) is resonant with the cavity mode. The joint atom–cavity states are the dressed states [7], $|\pm, n\rangle = (|e, n-1\rangle \pm |g, n\rangle)/\sqrt{2}$, superpositions of the degenerate uncoupled states $|e, n-1\rangle$ and $|g, n\rangle$. The energy splitting between these dressed states is $\hbar\Omega\sqrt{n}$, where $\Omega/2\pi = 50$ kHz is the vacuum Rabi frequency [Fig. 2(b)].

We make use of a third circular level h (principal quantum number 49), which is impervious to the interaction with the cavity mode, the $h \to g$ transition at 54.3 GHz being far off-resonance from the mode. The $|h, n\rangle \to |+, n\rangle$ transition frequency depends upon n. We can thus tune the source S to selectively address the transition with $n = s$. Note that the transitions corresponding to adjacent n values are detuned by a few kiloHertz only. The interrogation time should be long enough to resolve these levels. Slow atoms are thus mandatory, as well as carefully optimized interrogation pulses [21].

In the standard implementation of QZD, we would perform a π Rabi pulse on the $|h, s\rangle \to |+, s\rangle$ transition and then detect the atomic state by the destructive field-ionization method. An atom found in h indicates that the field does not contain s photons, a detection in e or g means that there are s photons in the cavity. However, the destruction of the atom is not mandatory, since the measurement result need not be read out to implement QZD.

It has been shown theoretically [14] and experimentally [26] that QZD can be implemented in three equivalent ways. It is obtained by the measurement of an observable with degenerate eigenspaces, or by the repeated application of a unitary operator having the same eigenspaces (in close relation with the 'Bang–Bang' control methods [27]), or finally by
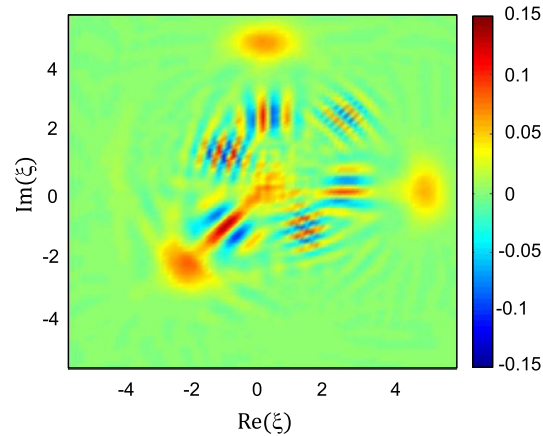
Fig. 3. Final-state Wigner function $W(\xi)$ after the synthesis of a complex state superposition. See text for the conditions. Reprinted from [21].

the continuous application of an Hamiltonian with again the same eigenspaces. All of these operations leave a quantum state localized in one of the eigenspaces unchanged, while the coherence between different eigenspaces is altered.

We can thus equivalently perform a 2π pulse on the $|h, s\rangle \rightarrow |+, s\rangle$ transition. It results in the transformation $|h, n\rangle \rightarrow (-1)^{\delta_{ns}}|h, n\rangle$. The atom always ends up in h, and is ready for another interrogation, while the field experiences a unitary 'kick' $U_s = 1 - 2|s\rangle\langle s|$, with the same degenerate eigenspaces as P_s.

QZD can be generalized to ECs centered at an arbitrary point γ in phase space by displacing the whole phase space by an amplitude $-\gamma$ before the 2π interrogation pulse, and by displacing it again by γ after the interrogation (these displacements are also performed by S'). This implements a kick operator $U_s(\gamma) = D(\gamma)U_sD(-\gamma)$.

This process naturally leads to the notion of phase-space tweezers [20]. Using a radius-one EC centered at the amplitude γ, we can freeze the evolution of a single coherent component, realizing a 'displaced QZE'. Even in the absence of externally driven dynamics, we can move this coherent component by adiabatically changing the position of the EC from one interrogation to the next. We can, for instance move at will separately the two components of a Schrödinger cat state.

More generally, the phase space tweezers lead to a state synthesis procedure [21]. Starting from the vacuum state, we first cast the interrogation atom in a superposition of h with an inactive state i (for instance, the circular state with principal quantum number 52, lying above e), which does not take part in the QZD process. We then perform a tweezers operation leading from the vacuum to a first amplitude, α_1. Since i is a spectator state, we indeed perform a quantum superposition of the tweezers operation and no operation at all. The atom gets entangled with a field involving a superposition of the vacuum with a displaced coherent component. Performing a partial transfer from i to h and resuming the operation from the vacuum part of this state, we create a second coherent amplitude α_2. An iteration of the process prepares an arbitrary superposition of non-overlapping coherent components.

Fig. 3 presents the Wigner function resulting from a numerical simulation of the process with the target state $\left(|4\rangle + |4i\rangle + |3e^{i5\pi/4}\rangle + |0\rangle\right)/2$. All tweezers actions are performed with a 0.1 amplitude increment between interrogations. The fidelity with respect to the target state is 99%.

QZD in cavity QED is within reach of the parameters of the planned experiment [Fig. 2(a)] [21]. Note that a closely related experiment has been recently realized in the circuit QED context (B. Huard, private communication). We devote the next section to an earlier experiment implementing QZD in a high-dimensional Hilbert space.

3. QZD in a Rydberg state manifold

We implement QZD [25] in a subspace of the Rydberg manifold with principal quantum number $n_e = 51$. This manifold contains ≈ 2500 levels, whose degeneracy is partially lifted in presence of a static electric field $\mathbf{F}$, defining the quantization axis Oz. The Stark levels are schematically represented in the center part of Fig. 4(a), sorted according to their magnetic quantum number m selected to be positive. They arrange in a triangular shape, with the circular state at its tip (thickest line).

A σ_+-polarized radio-frequency (RF) field couples the circular state with a ladder of nearly equidistant levels (thick lines), connected by transitions at the Stark angular frequency $\omega_a = (3/2)n_e ea_0 F/\hbar$ (a_0: Bohr radius, e: charge quantum). The atom being initially in the circular state, it evolves under the action of the RF field within a ladder of 51 levels, $|n_e, k = 0\rangle \ldots |n_e, k = 50\rangle$, where $|n_e, k = 0\rangle$ is the circular state. These levels are equivalent to those of a spin $J = 25$ in a magnetic field. They are represented in Fig. 4(b) as thin black lines, labeled by the quantum number k.

Note that, close to the top (as well as close to the bottom) of its energy ladder, a spin is equivalent to a harmonic oscillator. For small k values, the atom thus evolves in a Hilbert space equivalent to that of the cavity mode considered in the previous section, k playing the role of the photon number: The experiment performed here can be viewed as a quantum simulation of the CQED proposal.
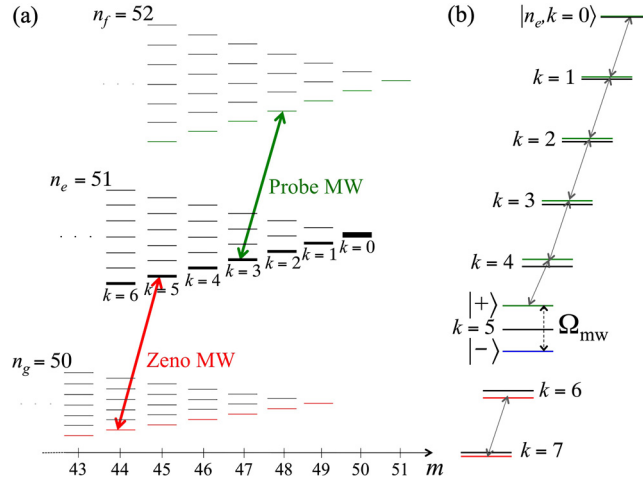
Fig. 4. Rydberg energy levels (a). Stark manifolds with principal quantum numbers $n_g = 50$, $n_e = 51$ and $n_f = 52$ (not to scale). The thick lines represent the spin states ladder coupled with the circular state $|n_e, 0\rangle$ (thickest line) by the σ_+ RF field. The green and red arrows show the transitions resonant with the probe pulse for $k_p = 3$, and with the Zeno MW for $k_z = 5$, respectively. (b) Spin states without (black lines) and with (colored lines) the Zeno MW. Reprinted from [25].

The evolution of the atom driven by a resonant RF field is a rotation of the spin, represented qualitatively as a classical vector on a generalized Bloch sphere (with the circular state at the North pole and the bottom state of the ladder at the South pole). The spin is, at any time, in a Spin Coherent State (SCS), whose average energy corresponds to the vertical position of the Bloch vector.

We have first investigated this unrestricted evolution. The atoms are prepared by laser excitation of a thermal atomic beam in a cavity-like structure, similar to that presented in Fig. 2(a) (the mirrors used here have a low reflectivity and the field modes they sustain, detuned from the atomic transitions, do not play any role). The static field $\mathbf{F} = 2.35$ V/cm is applied across the mirrors. The resulting Stark frequency is $\omega_a/2\pi = 230$ MHz. The eight electrodes circling the space between the edges of the mirrors are driven by RF generators. After optimization of their phases and amplitudes, we realize near the center of the structure a field with a σ_+ polarization (95% purity). At the start of the experimental sequence, we use a circularization process based on an adiabatic RF transfer to prepare the initial circular state from an optically accessible level.

We have measured, as a function of the interaction time t_1 with the RF, the probabilities $P(k_p, t_1)$ ($k_p = 0 \ldots 5$) for finding the atoms in the first levels of the spin ladder. These levels cannot be directly resolved by the final field ionization detection. We thus send, after time t_1, a probe microwave (MW) pulse tuned to resonance on a transition towards the $n_f = 52$ manifold [Fig. 4(a)]. The transitions originating from levels with different k values are easily resolved, due to the difference in the linear Stark polarizabilites (proportional to the principal quantum number) in adjacent manifolds. With a π probe MW pulse, we can thus selectively measure the population of any $|n_e, k_p\rangle$ level.

Fig. 5(a) presents the observed evolution of $P(k, t_1)$ for $k \leq 5$, together with snapshots of the probability distribution shown as histograms on the right. We clearly monitor a cascade down the spin states ladder. The observed data (points) are in excellent agreement with the SCS evolution, computed here with the RF-induced Rabi frequency $\Omega_{\mathrm{rf}}/2\pi = 152 \pm 4$ kHz as the main adjustable parameter. This unrestricted dynamics on the Bloch sphere is nearly identical to the displacement of the vacuum state close to the origin of phase space for a cavity mode.

QZD can be implemented by repeatedly asking the spin: "Has your projection on the polar axis of the Bloch sphere reached a specific value or not?" This specific value corresponds to a well-defined "limiting latitude" (LL) on the Bloch sphere. The spin is forbidden to cross the LL and its motion remains confined on the North polar cap. The LL plays on the Bloch sphere the role of the EC in the cavity mode phase plane.

To perform this interrogation, we use a state-selective MW transition towards the $n_g = 50$ manifold [Fig. 4]. We tune a continuous 'Zeno' MW source on resonance with a selected $|n_e, k_z\rangle \rightarrow |n_g, k_z\rangle$ transition. This resonant drive mixes the two levels into dressed states $|+\rangle$ and $|-\rangle$ separated by the MW Rabi frequency $\Omega_{mw} = 3.4$ MHz. This dressing opens a gap in the spin states ladder for $k = k_z$ and slightly shifts the other, nonresonant levels, as shown in Fig. 4(b). Note that we use here the continuous addressing version of the QZD instead of the bang–bang approach of the previous section. Both methods have been shown to be fully equivalent [14].

The RF drive is too weak ($\Omega_{rf} \ll \Omega_{mw}$) to jump this gap. Starting from the circular state, the evolution is confined to the states with $k < k_z$ and to the state $|+\rangle$, which can be reached trough a nearly resonant step due to the light shifts induced by the Zeno MW. Levels $|-\rangle$ and below are never reached. Switching off adiabatically the Zeno dressing maps the $|+\rangle$ state onto $|n_e, k_z\rangle$ [25]. The QZD thus effectively splits the angular momentum Hilbert space into $\mathcal{H}_N$, made up of the $k_z + 1$ levels with $k \leq k_z$ close to the North pole of the Bloch sphere, and the complementary southern subspace $\mathcal{H}_S$.
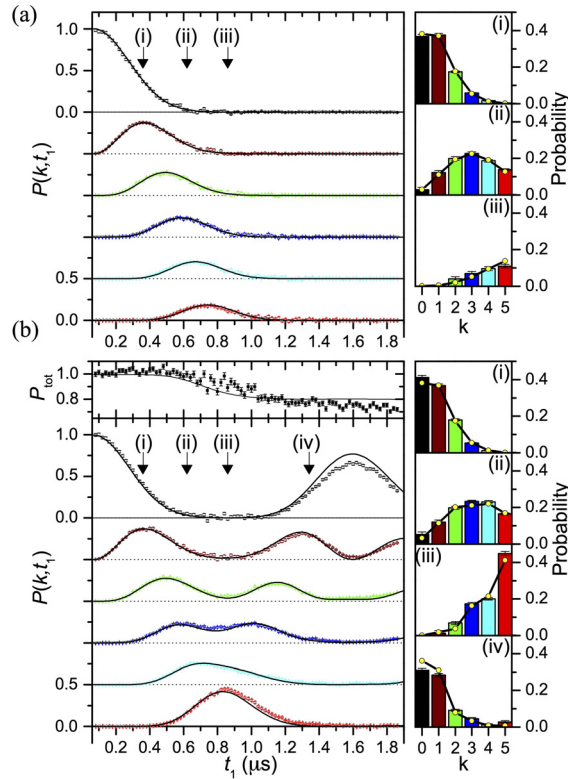
Fig. 5. Evolution of the spin state populations. (a) $P(k, t_1)$ for $k \leq 5$ in a free RF-induced rotation (no Zeno MW applied). The points are experimental with statistical error bars. The solid lines correspond to a fit on spin coherent state. The insets give the color code for the different k_p values and present the experimental histograms of $P(k, t_1)$ for three t_1 values (arrows in the main frame), together with the expected SCS distribution (solid lines). (b) $P(k, t_1)$ for $k \leq 5$ in a QZD with $k_z = 5$. The lines result from a complete numerical simulation of the experiment. The insets give the observed $P(k, t_1)$ distribution at four t_1 values (arrows in the main frame) together with the numerical predictions (solid lines). Reprinted from [25].
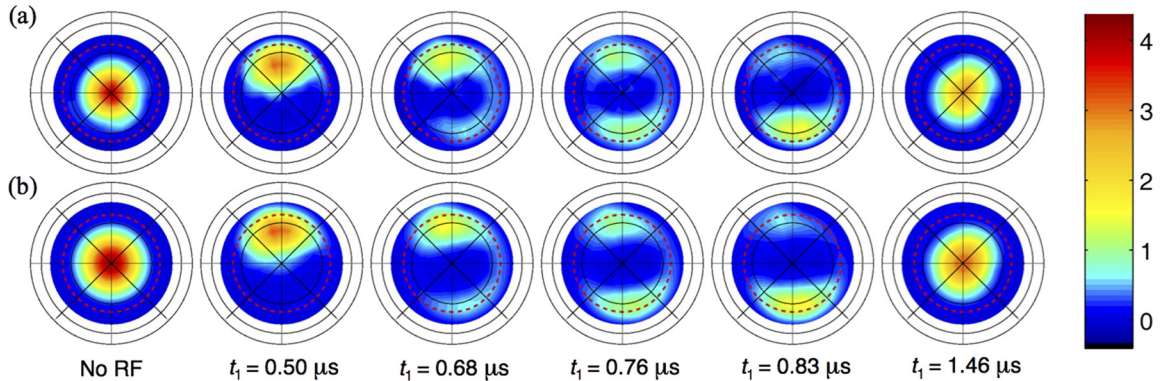
Fig. 6. Evolution of the Q function under QZD. (a) Measured $Q(\theta, \phi)$ functions for $k_z = 4$ on the Bloch sphere, represented in polar projection. The black thin lines indicate eight meridians and parallels separated by 15 degrees. Left frame: initial $|n_e, k = 0\rangle$ state (no RF rotation). The other frames correspond to increasing times from left to right, whose precise values are given below panel (b). The QZD motion is confined inside the limiting latitude (dashed red circle). (b) Corresponding numerical predictions. Reprinted from [25].

After a RF-induced QZD lasting a time t_1, we probe the level populations in $\mathcal{H}_N$. Fig. 5(b) presents the results for $k_z = 5$. The state distribution now bounces off a 'wall' at $k = k_z + 1$ and nearly returns to the initial state after 1.7 μs. This dynamics is drastically different from the runaway process observed without Zeno MW [Fig. 5(a)]. It is in excellent agreement with a complete numerical simulation of the experiment based on the independently measured experimental parameters (solid lines). The top frame shows the total population in $\mathcal{H}_N$. It drops by ∼20% at the bouncing time. This loss is mainly due to a residual transfer into $\mathcal{H}_S$ through the Zeno barrier.

We get a clearer picture of the states generated in the QZD by a direct measurement of the spin's Q-function. It is defined as $Q(\theta, \phi) = \langle n_e, 0|R^\dagger(\theta, \phi)\rho R(\theta, \phi)|n_e, 0\rangle$, where ρ is the angular momentum density operator and R the rotation
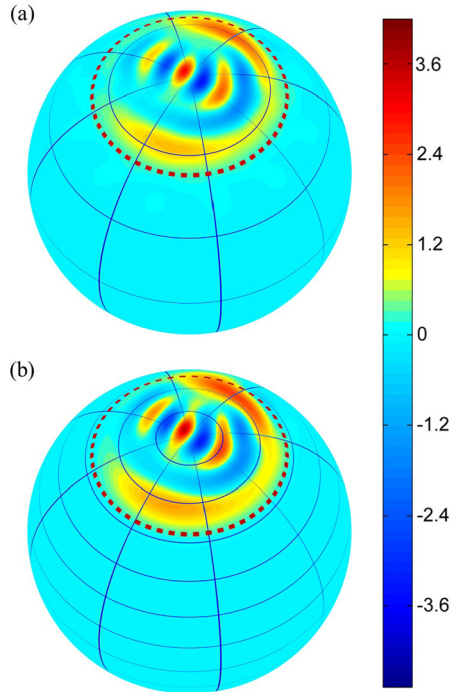
Fig. 7. Wigner function of the spin cat state. (a) Experimental Wigner function, $W(\theta, \phi)$, obtained from the reconstructed density matrix ρ of the spin after a QZD at the phase inversion time (fourth frame in Fig. 3). (b) Result of the numerical simulation of the experiment. Reprinted from [25].

along a meridian of the Bloch sphere bringing the North pole in the direction defined by the polar angles θ and ϕ. The Q-function is conveniently measured by performing at the end of the experiment a fast RF-induced rotation followed by a MW probe pulse measuring the population of the $|n_e, 0\rangle$ state.

Fig. 6(a) presents snapshots of the evolution. Starting from the North pole of the Bloch sphere, the spin state moves first 'upwards' until it reaches the LL. It then undergoes a phase inversion and is transiently cast in a state in which it points in two opposite directions at the same time. It then resumes its motion in the 'upwards' direction, returning to the North pole at the end of the sequence. This confined motion is quite similar to the one of the field in the previous section [Fig. 1(a)]. Fig. 6(b) presents the results of a numerical simulation of the experiment taking into account all known imperfections. The agreement with the observed data is excellent.

At the phase inversion time, we have checked the coherent nature of the spin state superposition by measuring the full atomic density matrix ρ. We perform, as before, a controlled RF-induced rotation of the spin at the end of the sequence. We then measure the populations of the first six spin states. From these data, we reconstruct ρ by a maximum-likelihood procedure. We display the result using the spin's Wigner function on the Bloch sphere, which is quite analogous to the field's Wigner function in the phase plane.

Fig. 7(a) shows this function at the phase inversion time. The interference fringes between the two coherent-like components give a vivid evidence of the non-classicality of this atomic state. The results of the numerical simulation are plotted in Fig. 7(b). Here again the agreement is excellent (93% mutual fidelity).

4. Conclusion and perspectives

We have discussed two closely related implementations of QZD. In the atomic case, we realize a confined quantum dynamics for a large spin isolated in the Stark Rydberg manifold. We observe the transient deterministic generation of nonclassical states, quantum superpositions of spins pointing in different directions. This realization opens interesting perspectives. With a better static field homogeneity and longer coherence times, we could create even larger cats. We also envision the application of quantum control techniques to prepare, for instance, a superposition of two circular states orbiting in opposite direction, or a superposition of two low-m states with opposite electric dipoles. The former is very sensitive to magnetic perturbations, the latter to electric ones. These state superpositions thus open the way to quantum-enabled metrology of weak fields.

QZD in a cavity offers even more promising perspectives. It makes it possible to prepare deterministically nearly arbitrary states, an interesting step for fundamental studies of the decoherence process. We could even envision coupling the rich structure of the Stark manifold to that of the cavity and to map an atomic state on a field one. The realization of a few-qubit processor with a single (natural or artificial atom) in a cavity is within reach.

S. Gleyzes, J.-M. Raimond / C. R. Physique 17 (2016) 685–692

Acknowledgements

References

[1] W. Zurek, Quantum Darwinism, classical reality and the randomness of quantum jumps, Phys. Today 67 (10) (2014) 50.
[2] M.A. Nielsen, I.L. Chuang, Quantum Computation and Quantum Information, Cambridge University Press, Cambridge, UK, 2000.
[3] R. Blatt, C.F. Roos, Quantum simulations with trapped ions, Nat. Phys. 8 (2012) 277–284.
[4] I. Bloch, J. Dalibard, S. Nascimbene, Quantum simulations with ultracold quantum gases, Nat. Phys. 8 (2012) 267–276.
[5] A.A. Houck, H.E. Tureci, J. Koch, On-chip quantum simulation with superconducting circuits, Nat. Phys. 8 (2012) 292–299.
[6] V. Giovanetti, S. Lloyd, L. Marcone, Quantum-enhanced measurements: beating the standard quantum limit, Science 306 (2004) 1330.
[7] S. Haroche, J.-M. Raimond, Exploring the Quantum: Atoms, Cavities and Photons, Oxford University Press, Oxford, UK, 2006.
[8] E.M. Purcell, Spontaneous emission probabilities at radio frequencies, Phys. Rev. 69 (1946) 681.
[9] A. Reiserer, N. Kalb, G. Rempe, S. Ritter, A quantum gate between a flying optical photon and a single trapped atom, Nature 508 (2014) 237–240.
[10] K. Hennessy, A. Badolato, M. Winger, D. Gerace, M. Atature, S. Gulde, S. Falt, E.L. Hu, A. Imamoglu, Quantum nature of a strongly coupled single quantum dot–cavity system, Nature 445 (2007) 896–899.
[11] M.H. Devoret, R.J. Schoelkopf, Superconducting circuits for quantum information: an outlook, Science 339 (6124) (2013) 1169–1174.
[12] S. Deléglise, I. Dotsenko, C. Sayrin, J. Bernu, M. Brune, J.-M. Raimond, S. Haroche, Reconstruction of non-classical cavity field states with snapshots of their decoherence, Nature (London) 455 (2008) 510.
[13] B. Vlastakis, G. Kirchmair, Z. Leghtas, S.E. Nigg, L. Frunzio, S.M. Girvin, M. Mirrahimi, M.H. Devoret, R.J. Schoelkopf, Deterministically encoding quantum information using 100-photon Schrödinger cat states, Science 342 (6158) (2013) 607–610.
[14] P. Facchi, S. Pascazio, Quantum Zeno subspaces, Phys. Rev. Lett. 89 (2002) 080401.
[15] B. Misra, E.C.G. Sudarshan, Zenos paradox in quantum-theory, J. Math. Phys. 18 (1977) 756.
[16] W.M. Itano, D.J. Heinzen, J.J. Bollinger, D.J. Wineland, Quantum Zeno effect, Phys. Rev. A 41 (1990) 2295.
[17] C. Balzer, R. Huesmann, W. Neuhauser, P. Toschek, The quantum Zeno effect – evolution of an atom impeded by measurement, Opt. Commun. 180 (1–3) (2000) 115–120.
[18] O. Hosten, M.T. Rakher, J.T. Barreiro, N.A. Peters, P.G. Kwiat, Conterfactual quantum computation through quantum interrogation, Nature (London) 439 (2006) 949.
[19] J. Bernu, C. Deléglise, C. Sayrin, S. Kuhr, I. Dotsenko, M. Brune, J.-M. Raimond, S. Haroche, Freezing coherent field growth in a cavity by the quantum Zeno effect, Phys. Rev. Lett. 101 (2008) 180402.
[20] J.-M. Raimond, C. Sayrin, S. Gleyzes, I. Dotsenko, M. Brune, S. Haroche, P. Facchi, S. Pascazio, Phase space tweezers for tailoring cavity fields by quantum Zeno dynamics, Phys. Rev. Lett. 105 (2010) 213601.
[21] J.M. Raimond, P. Facchi, B. Peaudecerf, S. Pascazio, C. Sayrin, I. Dotsenko, S. Gleyzes, M. Brune, S. Haroche, Quantum Zeno dynamics of a field in a cavity, Phys. Rev. A 86 (2012) 032120.
[22] P. Facchi, D. Lidar, S. Pascazio, Unification of dynamical decoupling and the quantum Zeno effect, Phys. Rev. A 69 (2004) 032314.
[23] H. Nakazato, M. Unoki, K. Yuasa, Preparation and entanglement purification of qubits through Zeno-like measurements, Phys. Rev. A 70 (2004) 012303.
[24] X.-Q. Shao, H.-F. Wang, L. Chen, S. Zhang, Y.-F. Zhao, K.-H. Yeon, Distributed CNOT gate via quantum Zeno dynamics, J. Opt. Soc. Am. B 26 (2009) 2440–2444.
[25] A. Signoles, A. Facon, D. Grosso, I. Dotsenko, S. Haroche, J.-M. Raimond, M. Brune, S. Gleyzes, Confined quantum Zeno dynamics of a watched atomic arrow, Nat. Phys. 10 (2014) 715–719.
[26] F. Schäfer, I. Herrera, S. Cherukattil, C. Lovecchio, F. Cataliotti, F. Caruso, A. Smerzi, Experimental realization of quantum Zeno dynamics, Nat. Commun. 5 (2014) 3194.
[27] L. Viola, S. Lloyd, Dynamical suppression of decoherence in two-state quantum systems, Phys. Rev. A 58 (1998) 2733–2744.